Alma Mater Studiorum Università di Bologna
Archivio istituzionale della ricerca

The effects of in-plane shear displacements at the springings of Gothic cross vaults

(Article begins on next page)

06 May 2024

The effects of in-plane shear displacements at the springings of Gothic cross vaults

Carmela Carfagnini[1], Simonetta Baraccani[1], Stefano Silvestri[1], Dimitris Theodossopoulos[2]

[1]*Department DICAM, University of Bologna, Italy*

[2]*ESALA, Edinburgh College of Art, University of Edinburgh, UK*

Abstract

Extensive damages recorded during recent strong Italian earthquakes highlighted how vulnerable masonry vaults are and what deformations they receive from the rest of the building, which can be simulated as two phenomena: (i) a dynamic response of the vault itself, above the lateral walls and piers, and (ii) a pseudo-static response of the vault to imposed displacements at its springings, triggered by significant movement from the lateral walls and piers. This paper aims at improving knowledge in this field by simulating the first of these phenomena as static shear deformation at the springings. An experimental programme was set on a model of a typical quadripartite square Gothic cross vault (from the aisle of the Holyrood Abbey in Edinburgh). The test on a 1:4 scaled model had the shear displacement applied by moving two abutments in the longitudinal sense until failure, recording the crack pattern evolution and displacements of the ridges, identifying the diagonal cracks normal to the shear displacement that cause the damage and collapse in the vault. The crack pattern was validated with linear and non-linear numerical models, confirming particular observations like the uplift of the ridges and concentration of damage along the notional shear diagonal. Non-linear models are capable of capturing not only the crack pattern evolution, but also the vertical and horizontal displacements of the structure.

Key words

Masonry cross vault - Experimental test - Shear displacement - Springings

1 Introduction

Damages and collapses observed in Italian churches after many recent earthquakes (Umbria 1997, L'Aquila 2008, Emilia 2012) pointed out the vulnerability of their masonry cross vaults [1] (e.g. Saint Francis church in Assisi, San Marco church in Aquila, and the Modena Cathedral), so

understanding their behaviour is crucial for the assessment of the seismic safety of the entire structure [2], [3], [4]. However, the evaluation of their seismic response is quite complex and depends on several factors, such as understanding fully the three-dimensional geometry, determining the mechanical properties of the constituent materials and assessing the effect of the behaviour of the underlying vertical elements (lateral walls and piers).

A vault under earthquake excitation is subjected to two main phenomena:

- dynamic response of the vault itself to acceleration of its springings;
- pseudo-static response to displacements imposed at its springings from the horizontal movements of the structures underneath (walls and piers).

Several advanced computational techniques have been developed to investigate the weakness of arch and vault structures, including Limit Analysis, Trust Network Method, Finite Element Method and Discrete Element Method approaches [5], [6]. [7], [8], [9], [10],[11].

Many experimental studies have analysed the structural behaviour of arches and vaults under static [12], [13], [14], and seismic action, mostly focusing on the dynamic response, [15], [16],[17], while some have performed displacement-controlled tests at the springings [18], [19], [20], [21], [22].

Nonetheless, only few specific studies on the pseudo-static response of masonry cross vaults to imposed shear displacements at the springings (Figure 1a) are available in the scientific literature [22], [23],[24]. In a multi-nave church, such a shear deformation mechanism can occur due to the large difference in the lateral stiffness between the nave and the perimeter wall or the façade (Figure 1b). For instance, damages traced back to this mechanism were observed in the Modena Cathedral after the 2012 Emilia earthquake [4]. Rossi et al. (2014) [23] performed tests on a 1:5 scale model of a groin vault made of 3D printed plastic blocks with dry joints, by applying an incremental horizontal differential displacement between two couples of opposite abutments. Consequently, Gaetani (2016) [24] performed different experimental tests reproducing in-plane horizontal shear distortion and longitudinal opening/closing of the abutments on the above model [23]. In the shear test, the maximum force was attained at about 3% of the shear displacement-to-span ratio, a little more than half of its collapse value. Milani et al. [22] presents the simulation of a wide and diversified set of laboratory tests on a small-scale model (1:5) representative of a brick masonry cross-vault. The model is made by plastic blocks with dry joints. Two types of displacement/rotation controlled tests have been simulated: DSA (Direct Seismic Action), representative of the inertial horizontal actions induced by the earthquake, and ISA (Indirect Seismic Action), corresponding with shear displacements imposed at the abutments due to the differential deformations of masonry walls. ISA tests mainly showed the great ductility of the system, the maximum force being attained at about 3% of the displacement over span ratio.

This paper describes an experimental research that aims to starting understanding this pseudo-static response. The first stage discussed here is a test conducted on a Gothic cross vault from the aisle of the Holyrood Abbey church in Edinburgh (UK). The layout of the church and the geometry of the quadripartite vault are representative of a wide range of medium-sized Gothic churches and a detailed model of the vault exists that could be adapted to the aims of this project [25].

This model is a 1:4 scaled replica built with timber blocks and lime mortar and the shear displacement is applied by moving two abutments in the longitudinal axis until failure (Figure 1a). Linear and non-linear numerical simulations are performed to interpret further the results of the test and complete the insight to the phenomenon.


(a)   (b)
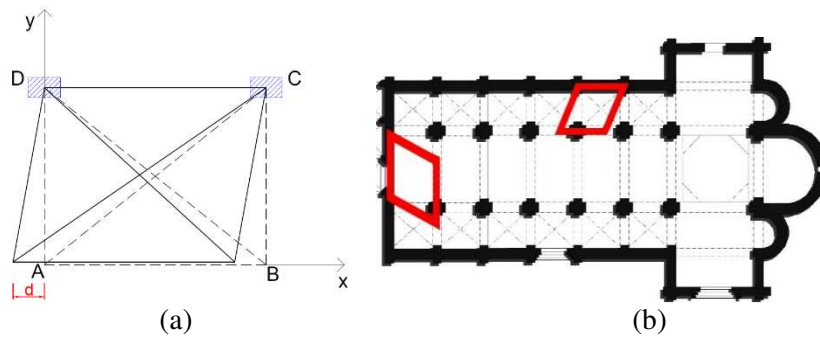
Fig. 1: *(a) Imposed shear displacements at the springings of a cross vault A and B against the stiffer edge C-D, (b) Origins in possible shear displacements in a church (e.g. plan view of the Modena Cathedral)*

2   The prototype vault from Holyrood Abbey

The vault investigated here is located on the surviving south aisle of the Holyrood Abbey church in Edinburgh. The church collapsed in 1768 after an unreasonable substitution of the decaying timber roof trusses with equally closely-spaced masonry walls which produced huge transverse thrusts that could not be contained by the badly maintained buttresses [26]. The performance of the vault in such conditions was studied earlier [19], [21] and the model from that research could be easily used for further studies on movement spread. The aisle vault considered is quadripartite and spans over an almost squared bay, with dimensions (4.9 x 3.78m and height of 3.03m) representative of many aisle vaults. While walls and piers were built with regular shaped stones, the vault webs are constituted in rubble masonry made of long thin blocks of irregular thickness (Figure 2a). The mechanical properties of the stone are assumed to be: (i) unit weight of 23.7 kN/m^3, (ii) elastic modulus 27.1 kN/mm^2 and (iii) compressive strength 42.8 N/mm^2[27].

The survey of the fourth bay vault highlights its typical proportions and particular geometrical characteristics. The longitudinal, nave arches are wide enough to support the lateral wall from the triforium and have a compound cross-section made of various deep mouldings. The ribs and the

transverse arches share the same plain cross-section. The transverse arches follow the quite typical proportions of an equilateral triangle, where the radius of the each of the generating half-arches is equal to the span of the arch (Figure 2b). The ribs use the same radius and they are almost semi-circular, as their centre is at the crossing of the diagonals of the bay.

(a)   (b)
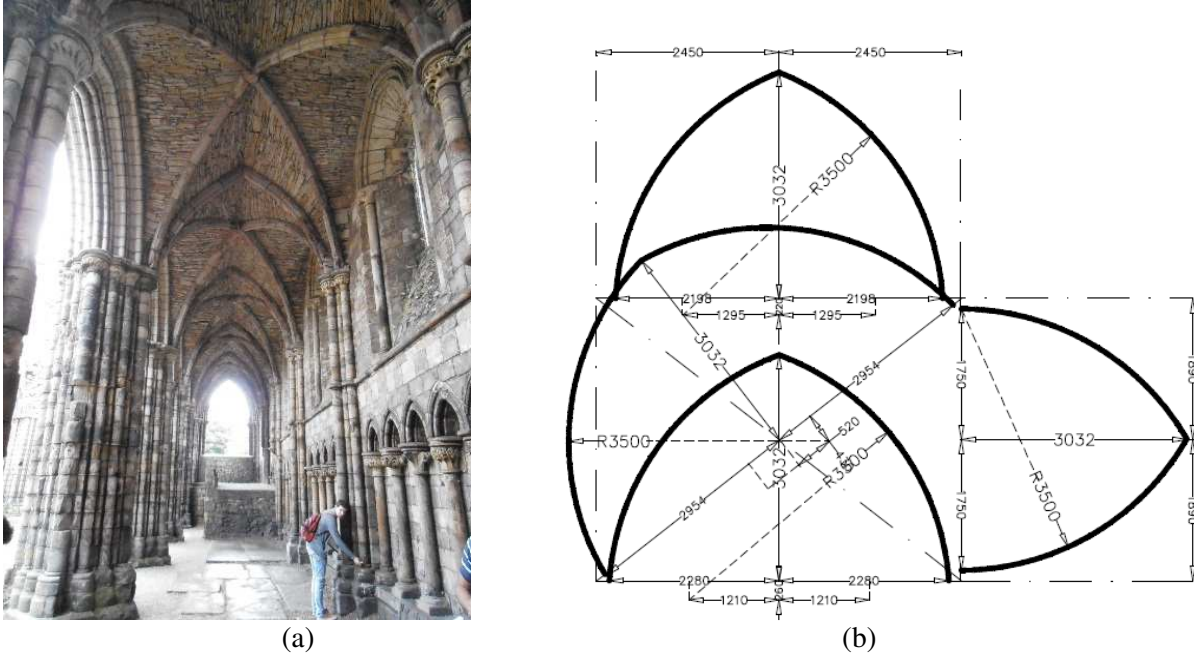
Fig. 2: (a) The South aisle of the Holyrood Abbey Church. (b) Measurements and proportions of the vault in the fourth bay of the south aisle - ground plan (dimensions in mm) [25]

3   The experimental programme on the scaled cross vault model

3.1   The model

The constructed physical specimen is a replica of the cross vault in ¼ scale (Fig. 2), with the following dimensions: the span of the transverse arches is 0.88 m, the span of the nave arch is 1.10 m, and the global rise is 0.76 m. Timber blocks were used to build the model [25], and bonding was achieved using a lime mortar mix. The advantages of using timber blocks were that the pieces could be produced very fast and the wood allows an accurate reproduction of the vault's shape and details. The mortar is a mix of one part lime and three parts sand, plus water and PVA glue, which creates a sufficient yet weak bond to allow failure to occur along the joints rather than the blocks [19].

The construction of the vault model is more extensively discussed in [28] and earlier in [19], [21],[25]. The nave, transverse and diagonal arches were built first as a form of skeleton and guide for the construction of the webs (Figure 3a).

Secondly, the webs were filled with timber blocks of uniform thickness. The blocks were cut and arranged to reproduce the masonry bond pattern and particular attention was paid to fit them along the ribs by forming a dihedral section specific for the end block of each row (Figure 3b).

(a)   (b)

Fig. 3: *(a) Construction of the vault arches.   (b) Timber blocks for the webs.*

The units were laid in rows for each web and were bonded with lime mortar. The construction started from the supports and each corner was built without falsework as the rows were quite vertical (Figure 4a), but a falsework was required when the row span and the web curvature increased (Figure 4b).

(a)   (b)

Fig. 4: *(a) Springing built without falsework.   (b) Plastic panels falsework for the subsequent courses.*

During this phase the arches work as a skeleton [12]: they provide the lateral support on which the extreme pieces of the rows are laid on. The falsework was removed carefully after the hardening of

the webs by lowering the supporting props. Figure 5 displays the completed model and the nomenclature used as reference to its structural elements.

(a)   (b)
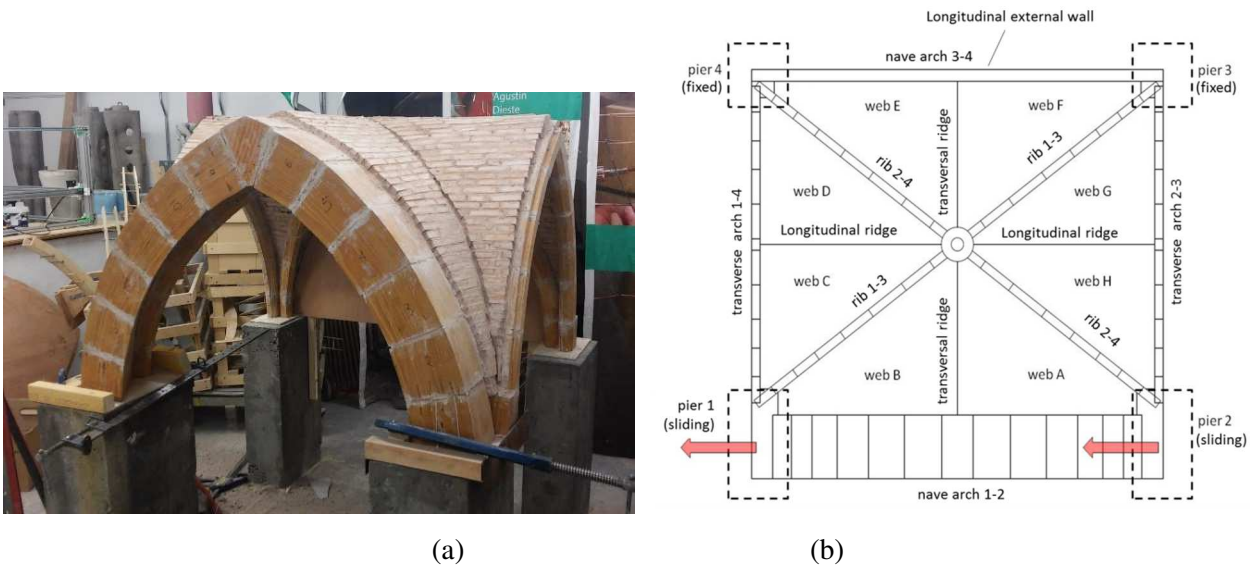
***Fig. 5** :(a) The model. (b) The nomenclature of the structural elements of the specimen.*

The vault was positioned above four stiff concrete piers. The two back springings were fixed to piers 3 and 4; the other two were fitted with a mechanism of moving along one direction to simulate the imposed shear displacement (piers 1 and 2). To form such a sliding mechanism, a plastic plate was fixed at the base of the springing, to permit sliding along a metal sheet laid on the piers. Guides were attached to control movement and avoid the sideways slipping of the supports. The longitudinal external wall of the Abbey was modelled using a panel with an arch shape and it was fixed on the two back piers with screws.

The strength of timber is lower than the stone one, but the cracks are supposed to occur along the joints only and they would not damage the blocks since the strength of the mortar is less than the timber's one, satisfying the typical assumptions introduced by Heyman [12]: infinite compression strength and negligible tensile strength of the masonry. For this reason, the results of the pseudo-static tests conducted on a scaled timber model may be considered dependent only on the geometry. From an engineering point of view, the findings could be thus used to understand not only the qualitative, but also the quantitative structural response of actual masonry vaults.

### 3.2   The shear displacement test

Shear displacement to the springings on piers 1 and 2 was applied manually through a turn-buckle connecting each springing to a steel stiff reaction frame (Figure 6a). Space displacements of

selected extrados points were recorded by a Total Station, positioned to capture as much extrados surface as possible (Figure 6b). In particular, points were chosen along the longitudinal and transverse ridges, the transverse arches and the nave arch, as well as on the front webs (namely, A, B, C and H).

(a)   (b)
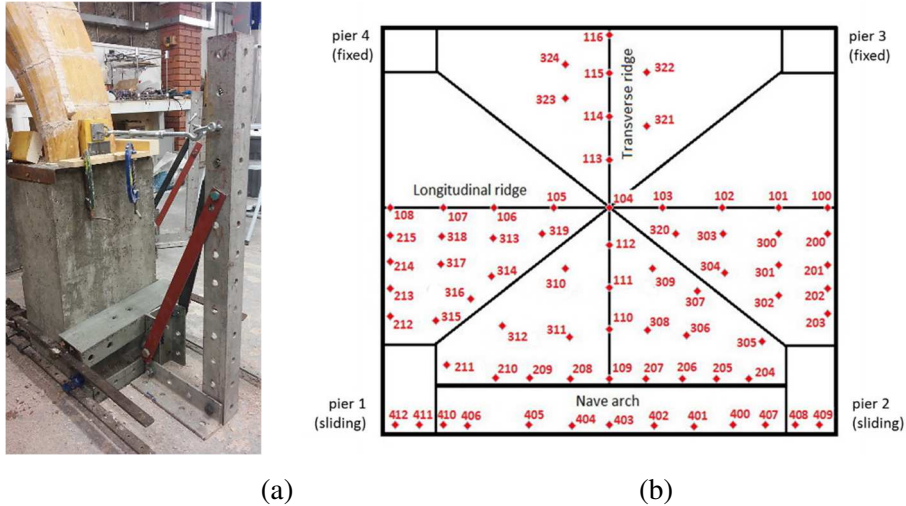
Fig. 6 *:(a) The turn-buckle connected to a rigid steel reaction frame.   (b) The position of the points monitored during the test.*

3.3   The test results

The crack pattern was recorded on the extrados and the intrados after every displacement increment [28]. Figure 7 displays the crack pattern at different shear displacement stages.

Cracks were observed immediately at the beginning of the test:

- at the 2 mm stage of shear displacement, bending cracks initiated at the extrados along the joints between the nave arches and web B, as also web F. Other "sliding" cracks (i.e. cracks associated to shear mechanisms) developed along the diagonal ribs, in particular on webs C and G;

- at 4 mm, a long bending crack was observed on the extrados of the longitudinal ridge. The earlier cracks propagated and additional small cracks appeared on the webs and along the transverse arches. A small hinge started to develop at the extrados of the two central voussoirs of the nave arch. Moreover, several cracks appeared at the intrados close to all the four springings;

- shear displacement at 10 mm caused the formation of new cracks. The transverse arch 1-4 showed the formation of one hinge in its central part. Two new bending cracks formed on webs C and B in correspondence to the initial "sliding" cracks. It should be noticed that these cracks, at 45° with respect to the diagonal rib 1-3, compromised the integrity of the rib itself, since they appeared across its section ;

7

- at 20 mm, the cracks along the nave arch and webs B and F widened and propagated, in particular in the extrados of web F and the intrados of web B reaching also web A. New cracks appeared at the extrados of the nave arch (indicating possible hinge locations). The 4 mm-crack along the longitudinal ridge of the web C significantly spread closer to rib 1-3;

- at 30 mm, long cracks developed on the extrados, in particular in webs H and F. On the extrados of the web F, the new crack ran across all the web, joining from rib 1-3 to nave arch 3-4 (Figure 8a). Another considerable crack formed at the intrados of web A close to the keystone. This scenario is to be considered as the failure of the vault in service or $30/1,100 = 1/37$ of the longitudinal span of the nave arch.

Figure 7 also displays the final crack pattern and the first partial collapse:

- during the 35 mm stage, partial failure of web F occurred (orange area in Figures 7 and 8b). The bigger crack at the 30 mm stage detached the voussoir on the rib 1-3 and this caused a rotation of the cracked web around the nave arch. A new long "sliding" crack also developed along the same rib on the intrados of the entire web C;

- during the last stages more damage occurred. At the shear displacement stage of 40 mm, the cracks along the ribs (webs C and E) and along the nave arch extended to the whole length on the extrados. New cracks developed at the intrados of web A and E close to the keystone;

- further increasing of the shear displacement up to 45 mm caused a partial collapse in web C (yellow area in Figures 7 and 8c). The nave arch looked very deformed and hinges are clearly recognizable (Figure 8d);

- the shear displacement stage of 55 mm caused the failure of the whole web B and the remaining part of web C (pink area in Figure 7);

- the shear displacement stage of 62 mm, corresponding to the last stage before the global collapse of the vault, provoked a detachment of a portion of the webs G and H close to the keystone.
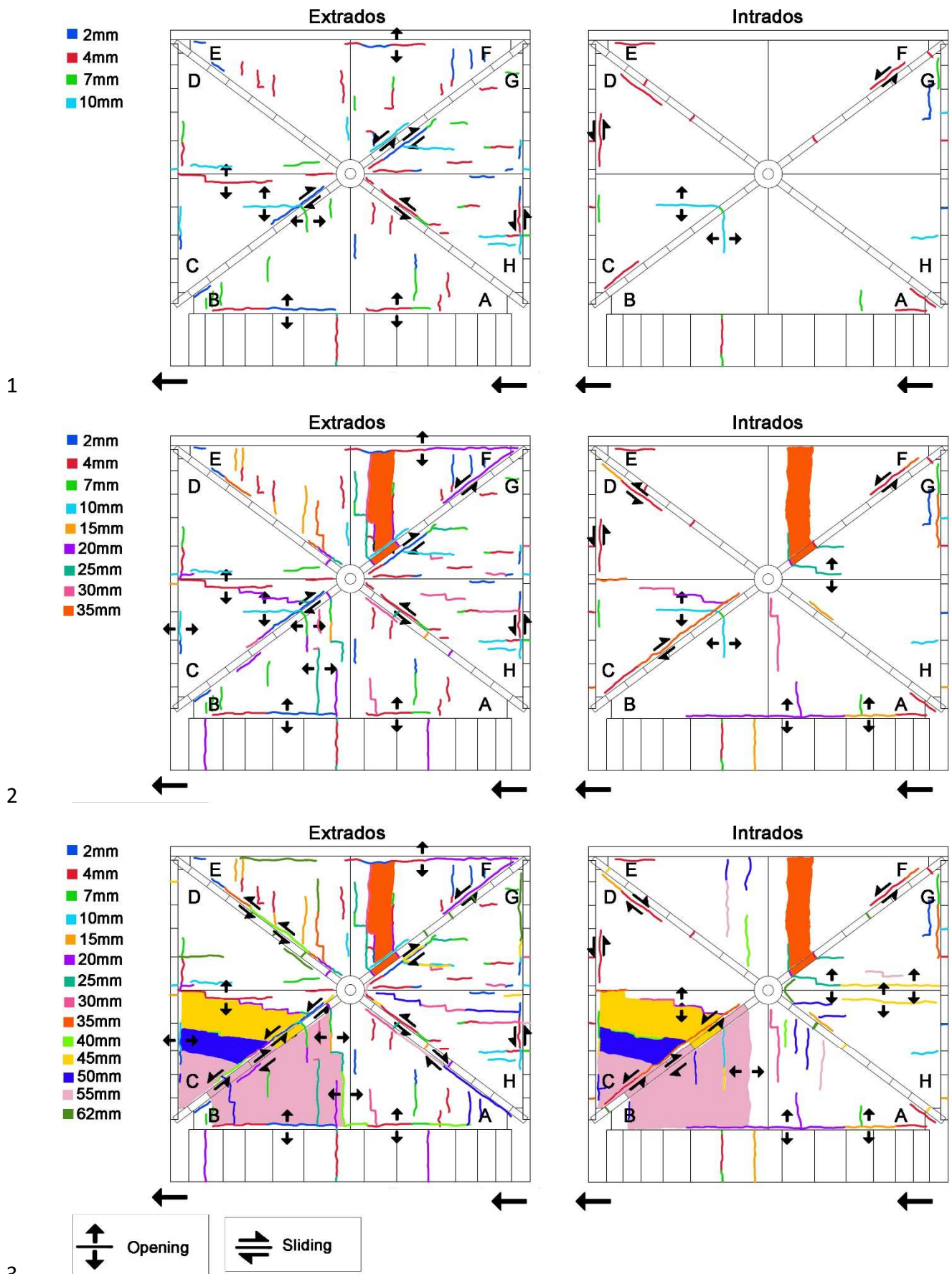
Fig. 7: *Crack pattern evolution and collapse condition.*

1

2

3   (a)   (b)

4

5   (c)   (d)

6   ***Fig. 8:** (a) The crack pattern at the shear displacement of 30mm, (b) Collapses at a shear displacement of*
7   *35mm, (c) Partial collapse at the 50 mm stage, (d) Hinges on the nave arch at 45mm.*

8

9   Table 1 and Figure 9 summarise the main effects observed on the model and provides

10   dimensionless shear displacement levels (with respect to the nave arch span 1.10 m) that can be

11   useful as a rough indication of the damage limits of similar cross vaults. The collapse mechanism in

12   Figure 9a can be summarised in these key stages: (1) diagonal cracks form, splitting along the bed

13   joints of the affected webs B, C, F and G; (2) shear detachment of the webs from the more rigid

14   edges (nave arch and wall); (3) these areas across the other diagonal are mainly in compression. The

15   arrows reported in Figure 9a represent the propagation direction of the cracks. Figure 9b shows a

16   basic model to understand the shear displacement from the deformation of the plan: the spreading

17   rib 1-3 still maintains its thrust line and opposes the outward deformation of rib 2-4 and of

18   transverse ridge. The hinges forming though in rib 1-2 join with the shear deformation of webs B,

19   C, F and G. Failure happens essentially at 3% spread of the longitudinal span. This is in good

20   agreement with results obtained by Gaetani (2016) [24], Rossi et al. (2014)[23], and Milani et al.

21   (2016) [22].

22

23

1

Table 1: *Summary of the cracking pattern stages.*

| Shear displacement stage	% Dimensionless shear displacement (with respect to the nave arch span)	Monitored effects on model
0 mm	0	-
4 mm	0.4 %	Formation of small cracks
10 mm	0.9 %	Initiation of major cracks in area 1
30 mm	2.7 %	Extension of the major cracks
35 mm	3.2 %	Partial collapse of webs
62 mm	5.6 %	Total collapse of the model

2

3

(a)   (b)
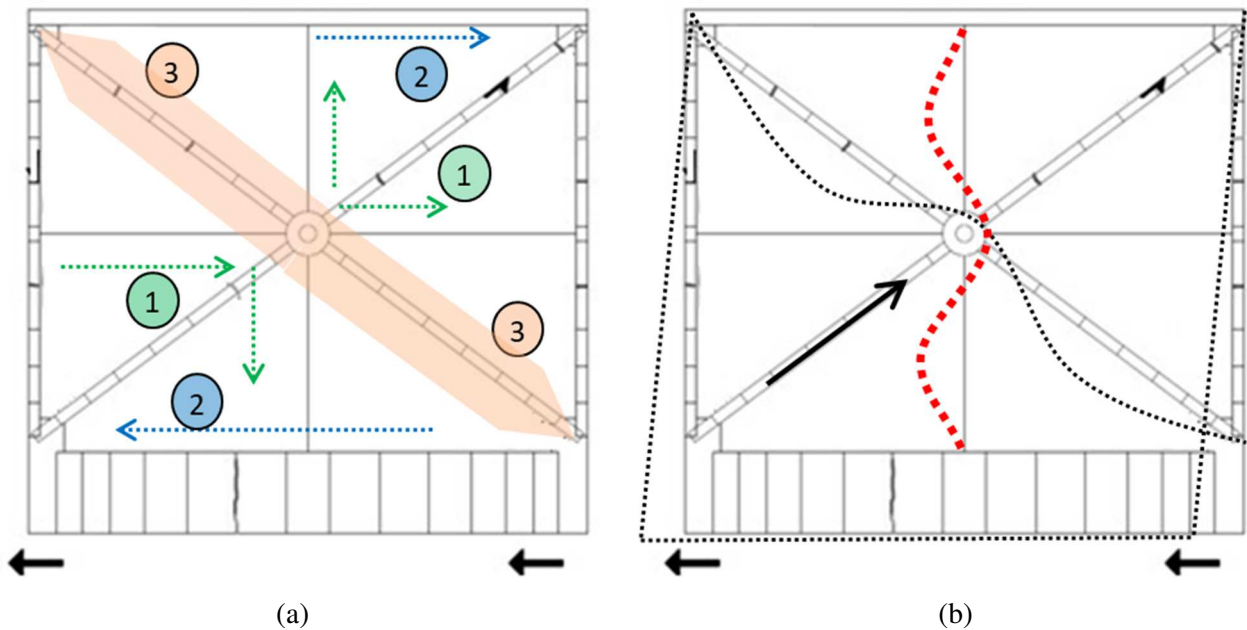
Fig. 9: (a) The failure mechanism of the vault model and observed stages.   (b) Reaction of rib 1-3 (black arrow) to the deformation of rib 2-4 (black dotted line) and to the deformation of transversal ridge (red dotted line) due to the shear displacement applied at the springings 1 and 2.

The displacements of the monitored points obtained via Total Station are hereafter illustrated with specific reference to the vertical and horizontal movements of the transverse ridge and the two diagonal ribs.

The vertical displacements of the transverse ridge are reported in Figure 10. It can be noticed that they increased upwards during the test and the final uplift of the keystone was 24 mm.

The horizontal displacements of the transverse ridge are reported in Figure 11. The general horizontal movement follows the imposed displacements at the springings, with the largest displacement in the front side (nave arch). The deformation looks like a rotation around the wall

11

1 edge 3-4 associated with the effects of the reaction of rib 1-3 next to the keystone (see also Figure

2 9b). The points are almost aligned for all the length of the transverse ridge except for the points

3 closer to the keystone which show a displacement in the opposite direction during the initial steps

4 of the test (probably due to the compressive action generated by rib 1-3).
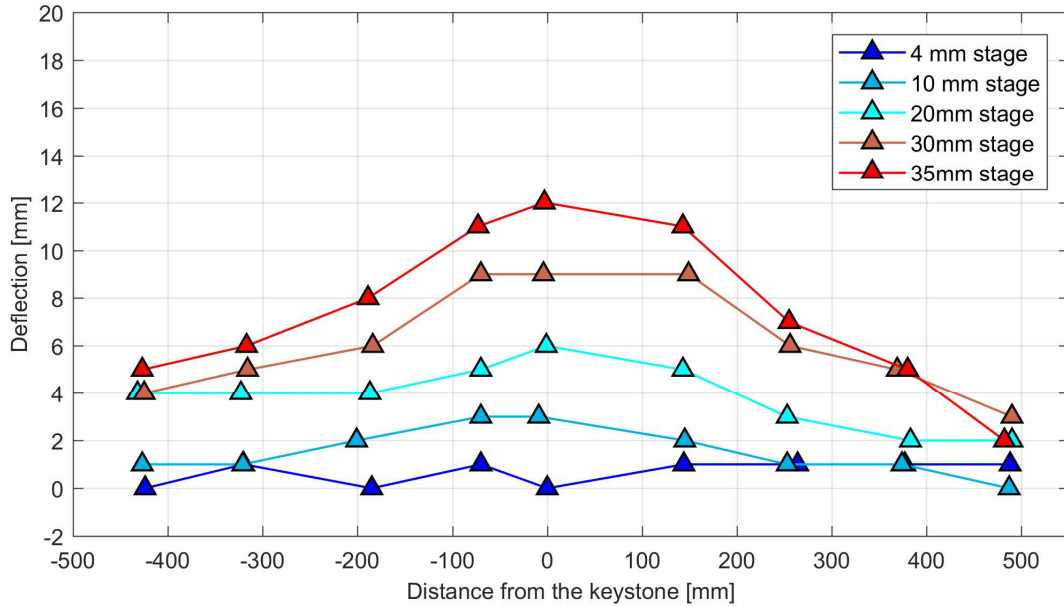
Fig. 10: *Upward vertical displacement of the transverse ridge*
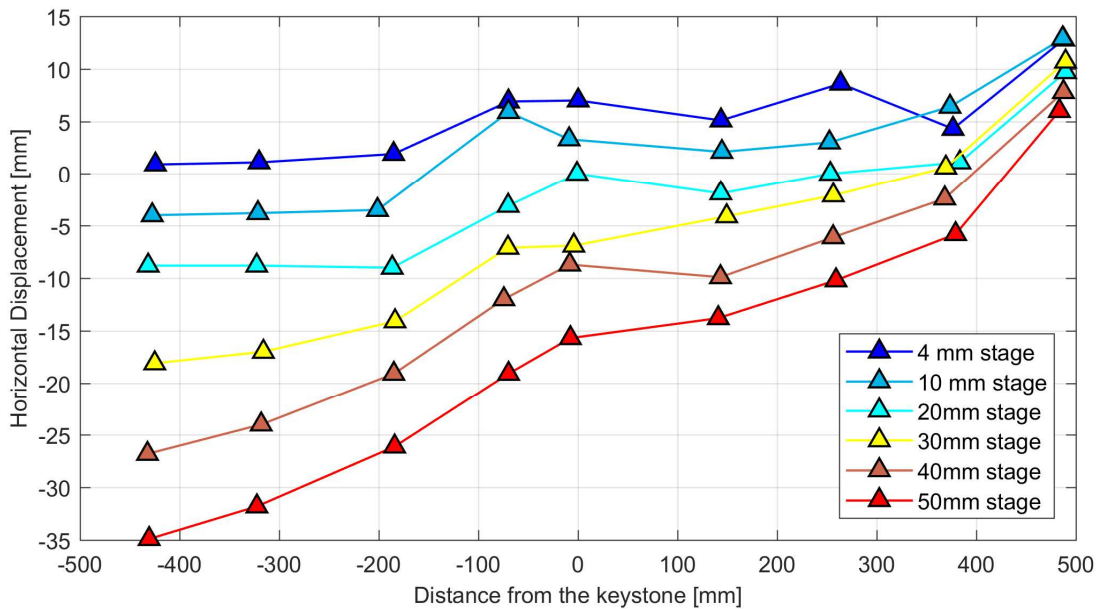
Fig. 11: *Horizontal displacement of the transverse ridge*
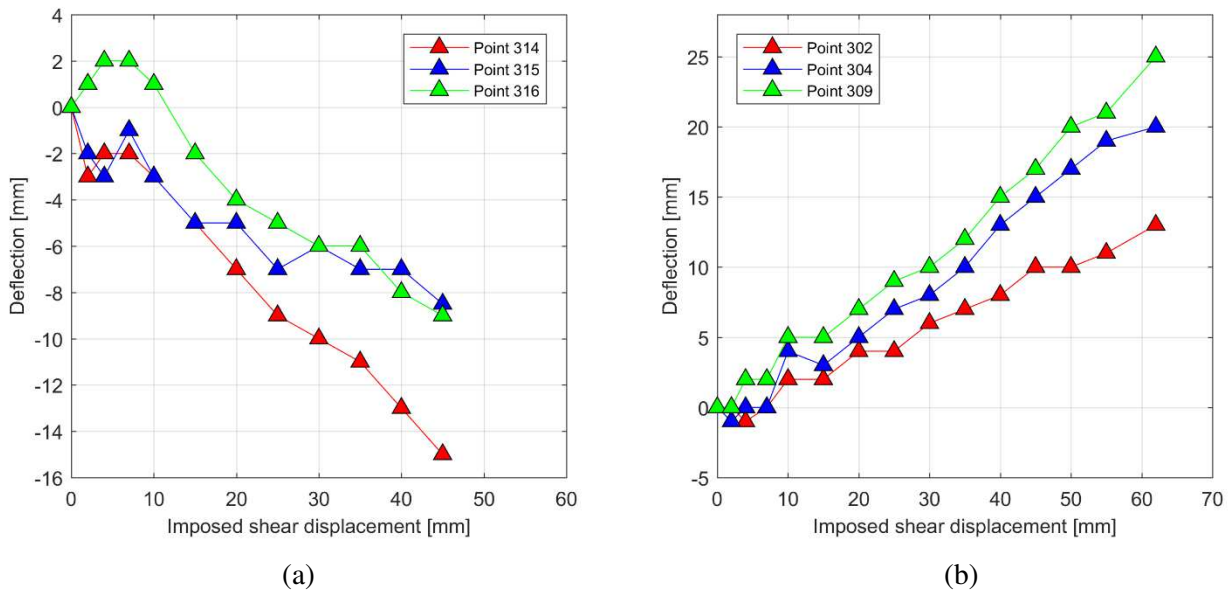
11 Similarly to the transverse ridge, the ribs moved horizontally in the same direction of the imposed

12 shear displacement. On the other hand, in the vertical direction, the points along rib 1-3 (spreading,

12

in tension) moved slightly downwards (Figure 12a), whilst the points along rib 2-4 (the one in compression) moved upwards (Figure 12b).

(a)   (b)

Fig. 12: *Vertical displacements of (a) rib 1-3 and (b) rib 2-4 during the test*

4   Reproduction of the experimental tests by means of a Finite Element model

The structural response of the cross vault timber-mortar model subjected to shear displacement at the springings has been also investigated by means of Finite Element (FE) models simulated in Abaqus v6.12, following a macro-modelling approach. With the purpose of identifying the simplest model capable of capturing the behaviour observed during the experimental test, a linear analysis has been first developed. The rationale behind the search for a simple model is to enable engineering practitioners to take advantage of the information presented in this research work, to compare and/or validate results from modelling similar masonry vaults. A simple model, nevertheless able to grasp the main issues, can be the robust basis for planning strengthening interventions and quickly evaluating their effectiveness. However, linear analyses have shown to be of limited validity for the study of masonry structures. Indeed, these analyses provided only an indication on the mechanical behaviour of the structure in the first stages of the test, assuming that the areas where high tensile stresses are concentrated represent the sections where the cracks first develop. However, they were not able to correctly reproduce the redistribution of stresses occurring at the movements of the vault. For instance, the experiment has shown an upward movement of the transverse and the longitudinal ridges, whilst an opposite trend (downward movement) has been obtained in the FE linear model. For this reason, the results of the linear analyses are not reported.

13

1 Only the results of the non-linear analyses considering the Concrete Damage Plasticity (CDP)

2 model to represent the constitutive behaviour of the timber-mortar material are presented hereafter.

4.1 The material properties

4 Vaults are expected to resist any bending that develops through their thickness and in ideal

5 conditions (e.g., specific geometries, perfect constraints, typical uniform static loads, …) they are

6 very stable under dead load, but it is well known that any discrepancy like imposed shear

7 displacement at its springings may lead to not negligible bending [29], [30].

8 The flexural stiffness and strength along the directions parallel to the bed joints (X) and normal to

9 the bed joints (Y) were evaluated through four-point bending tests on timber-mortar wallette

10 samples (Figure 13) [19], [25] and Table 2 collects the material properties obtained.

11

13   (a)   (b)   (c)
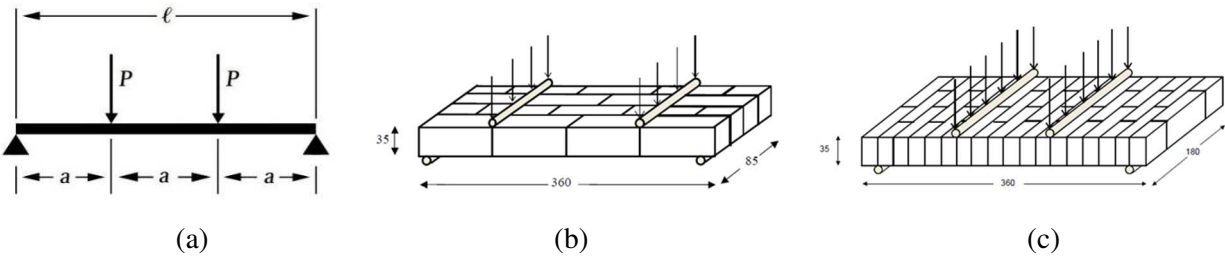
14 *Fig 13: (a) The 4-point wallette test; (b) direction X parallel to the bed joint (c) direction Y perpendicular to*
15 *the bed joints*

16

17 ***Table 2.*** *Material properties from flexural tests*

	Parallel to bed joints (X)	Normal to bed joints (Y)
Modulus of elasticity (N/mm^2)	4200	670
Flexural strength (N/mm^2)	0.98	0.32

18

4.2 The FE model

20 The FE model was discretized using quadrilateral shell elements for the webs and the large nave

21 arch, and beam elements for the transverse arches. In particular, the shells were modelled with

22 S4R5 elements in Abaqus, quadrilateral doubly-curved thin shells (with 5 degrees of freedom per

23 node), while the transverse arches were modelled with quadratic beam elements B21.

24 The mechanical properties in Table 2 were applied to the shell elements of the model. The

25 properties applied for every type of element are reported in Table 3.

26

27

28 ***Table 3****: Mechanical properties of the materials used in the finite elements.*

	E parallel to bed joints (X) (N/mm^2)	E normal to bed joints (Y) (N/mm^2)	υ_{12}	density (kg/m^3)	thickness (mm)
web shell	4200	670	0.2	700	35
nave arch shell	6000		0.2	700	160
beam	500		0.2	700	

Pinned connections were applied as the base constraints. Fixed supports were applied in the nodes of the wall edge to simulate the presence of the longitudinal external wall.

First, the self-weight (7 kN/m^3, to account for the timber blocks and the lime mortar) was applied to the model. Second, the shearing deformation was applied with displacements imposed in piers 1 and 2 along the negative X direction. The displacement was deployed in several steps until a total value of 100 mm to monitor the crack pattern evolution.

4.3 Non-linear analysis results

Non-linear static analysis was carried out for the interpretation of the experimental results. The analysis was performed reproducing the non-linear properties of the timber-mortar units with a smeared crack approach (the initiation of cracking process at any location happens when the material stresses reach one of the failure surfaces either in the biaxial tension region or in a combined tension-compression region) [33]. Timber-mortar units, as well as typical masonry brick-mortar units, are characterized by an orthotropic behaviour, which is difficult to model. Several researches focus on the identification of an orthotropic damage model able to represent the masonry structures [34], [35].

According to Roca et al. [6] and Lourenco et al. [36], two main modelling approaches based on FEM are available for masonry structures: (i) micro-modelling: units and mortar are represented as distinct elements and the unit-mortar interface are treated as discontinuous elements, and (ii) macro-modelling: units and mortar are homogenized in a continuum (isotropic or anisotropic) equivalent material. Several attempts to use brick-interfaces for the finite element modelling of masonry have been carried out [31], [32]. Macro modelling is probably the most popular and practical approach for the analysis of large structural members or full structures. However, constitutive models of the homogeneous material are difficult to be determined and have not been standardized yet. Several studies have suggested specific constitutive formulations for the analysis of masonry structures, considering different inelastic criteria for tension and compression and different hardening/softening behaviour along each material axis [31],[35], [37], [38], [34].

In the last decade, several studies have focused on homogenization procedures to take into account for the heterogeneity and anisotropy of the masonry material. The homogenization process consists

1   in replacing the repetition of a heterogeneous elementary cell through a homogeneous one whose

2   constitutive relationships are derived from the characteristics of its individual components [8], [10],

3   [11], [39]. However, in the scientific literature, the assumption of an isotropic concrete model has

4   proven to be able to reasonably predict the masonry behaviour as long as proper material definition

5   is provided [40], [41], [42], [43]. In this paper, as a preliminary study, the Concrete Damage

6   Plasticity (CDP) model was selected to model the constitutive behaviour of the timber-mortar

7   material. In detail, the CDP model is characterized by an isotropic constitutive law defined by

8   different strengths in tension and compression, an elasto-plastic behaviour with damage and a

9   softening phase ruled in tension and compression by two independent parameters and a 3D

10 behaviour obeying a Drucker-Prager failure criterion. The behaviour of the material is linear-elastic

11 up to a certain value, σ_{t0} for tension and σ_{c0} for compression (for the compressive branch there is an

12 additional stress increment due to hardening before reaching its peak stress value σ_{cu} and showing

13 compression crushing), thereafter the stress-strain curves drop down. The degradation of the elastic

14 stiffness on the strain softening branch of the stress-strain curve is characterized by two damage

15 variables, d_t and d_c, which can take values from zero (undamaged material) to one (which

16 represents the total loss of strength) [44], [45].

17 Considering Heyman's assumption of infinite compressive strength, generally adopted for masonry

18 structures and here assumed also valid for the timber units, the compression model parameters

19 reduce to the elastic modulus only since $d_c = 0$, whilst a full relationship should be defined for the

20 tension model accounting for the softening branch. All parameters were selected on the basis of the

21 four-point bending tests on wallettes (Figure 13 and Table 2). Elastic modulus in compression was

22 set to 4200 N/mm^2. Table 4 reports the stress-strain relationship in tension. The softening branch

23 has been assumed piece-wise linear from the max-strength point to a point obtained imposing a

24 reduced elastic module equal to 10% of the initial elastic module in correspondence of $\varepsilon = 0.002$.

25

26 *Table 4 Stress-strain relationship in tension*

Strain ε_t	Stress σ_t [N/mm^2]
0	0
0.00023	0.98
0.00200	0.84
0.0066	0.46
0.0098	0.19

27

28

Table 5 collects the main model parameters used in the non-linear analysis in agreement with literature recommendations [44], [46], [47], [48], [49].

Table 5 *Masonry parameters according to CDP*

Concrete Damage Plasticity	
Dilatation angle	10°
Eccentricity	0.1
σ_{b0}/σ_{c0}	1.16
Kc	2/3
Viscosity parameter	0.002

Figure 14 displays the tension damage variable (d_t) contour plots for the different shear displacement applied. It can be noticed there is a good agreement between the failure pattern obtained by the FE non-linear analysis and the cracks from the experiment. The non-linear analysis exhibits the first collapse ($d_t = 1$) at the 25 mm stage of shear displacement instead of the 35 mm stage obtained in the experiment.

The validation of the vertical displacements of the longitudinal ridge (Figure 15) shows that the non-linear simulation is capable of well reproducing the experimental responses at all stages of loading both qualitatively and quantitatively. In particular, contrary to the linear analysis, the vertical uplift is well captured by the non-linear simulations.
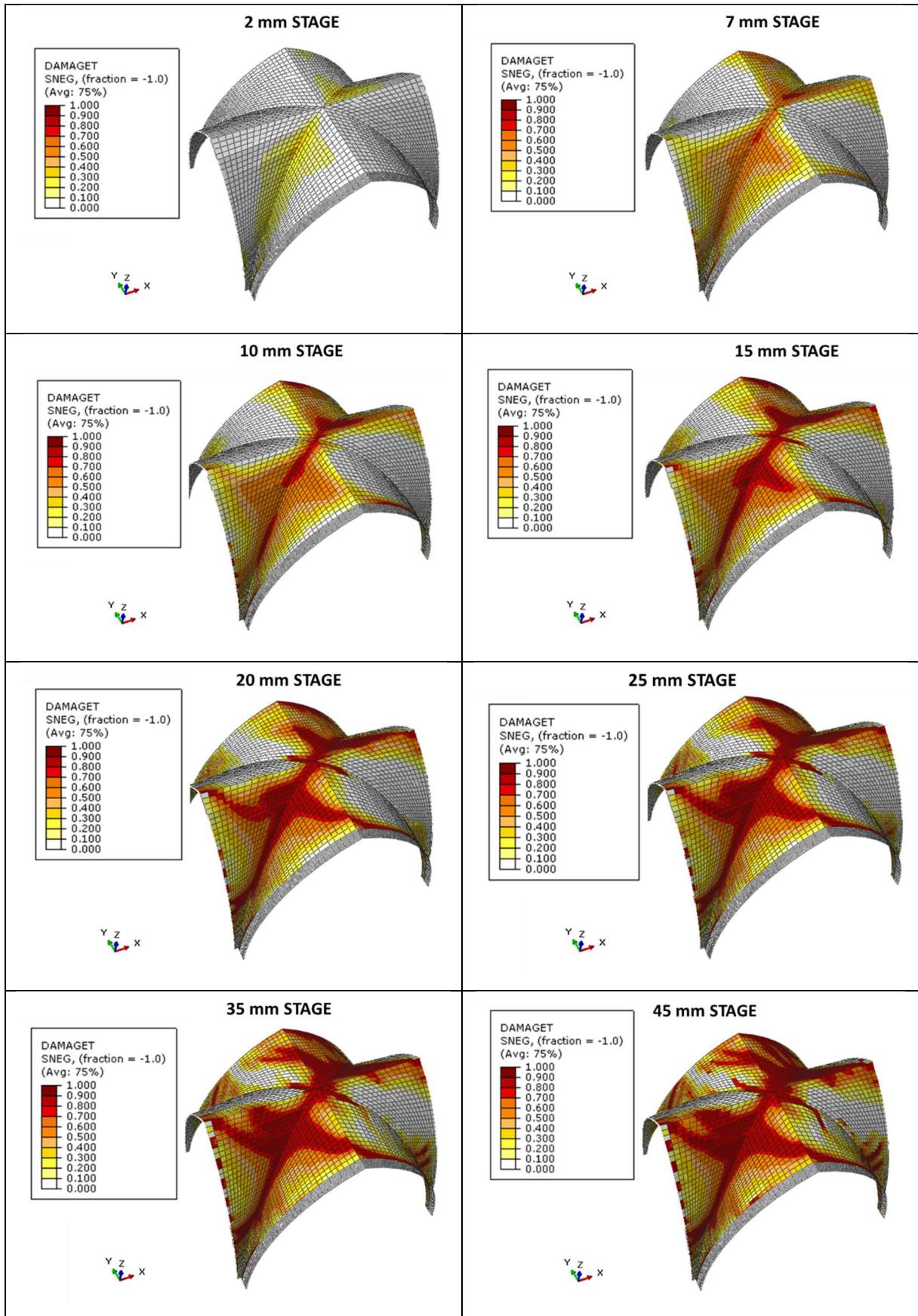
1

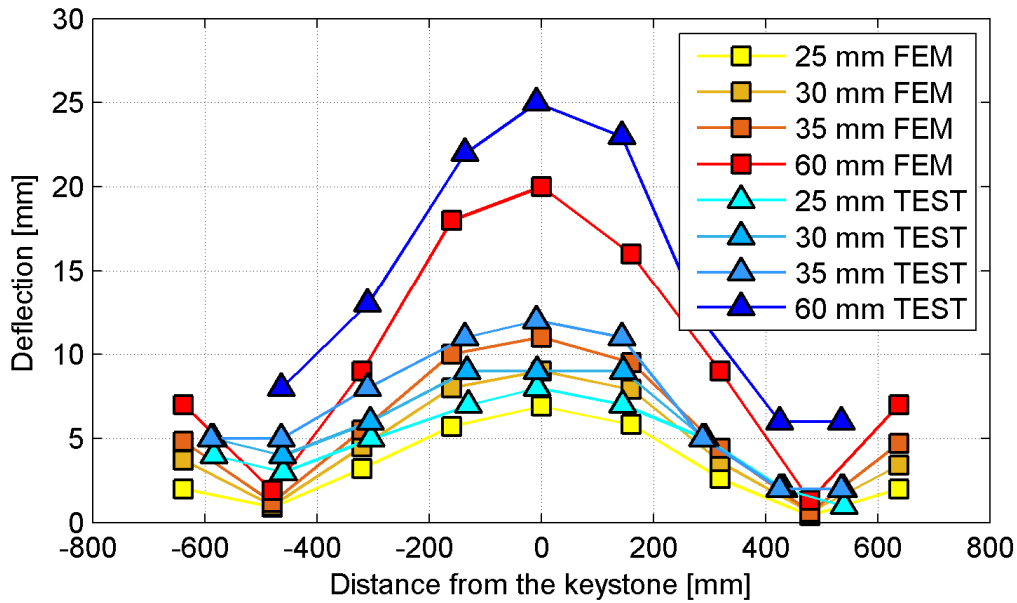**Fig. 14:** *Non-linear static damage contour plots*

2
3

18

1

*Fig. 15: Vertical displacement of the longitudinal ridge – Numerical and experimental results*

5 Comparison between experimental results and real-field data

This insight can be useful to interpret the crack pattern in the perimeter vaults of a church after an earthquake. For instance, this section presents a qualitative interpretation of the real crack pattern detected in the nave perimeter vaults of Modena Cathedral (Italy) after the 2012 Emilia earthquake. Figure 16 shows the cracking pattern of all cross vaults: the most damaged vault is the one of the nave connected to the façade (V1). This cross vault at the edge of the church is in the same boundary conditions as the tested one, as it has one side connected to a rigid wall and the other one subjected to shear transverse movements induced by the central body of the church. Figure 17 presents the first three ~~five~~ modes of vibration of the Modena Cathedral which highlight the tendency of the masonry churches to develop large transverse displacements of the central portion of the naves (associated with large out-of-plane movements of the perimeter walls).
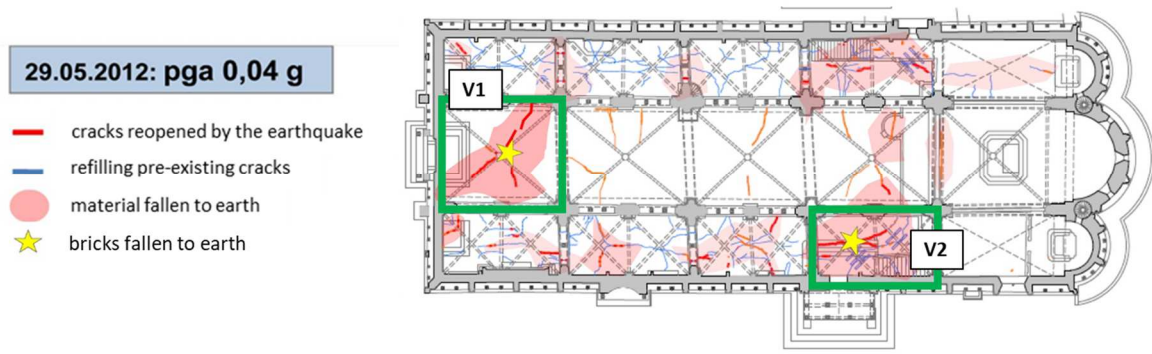
Fig. 16 *Post-earthquake crack pattern of the Modena Cathedral.*

$T_1 = 0{,}35$ s $\qquad\qquad T_2 = 0{,}31$s $\qquad\qquad T_3 = 0{,}28$ s
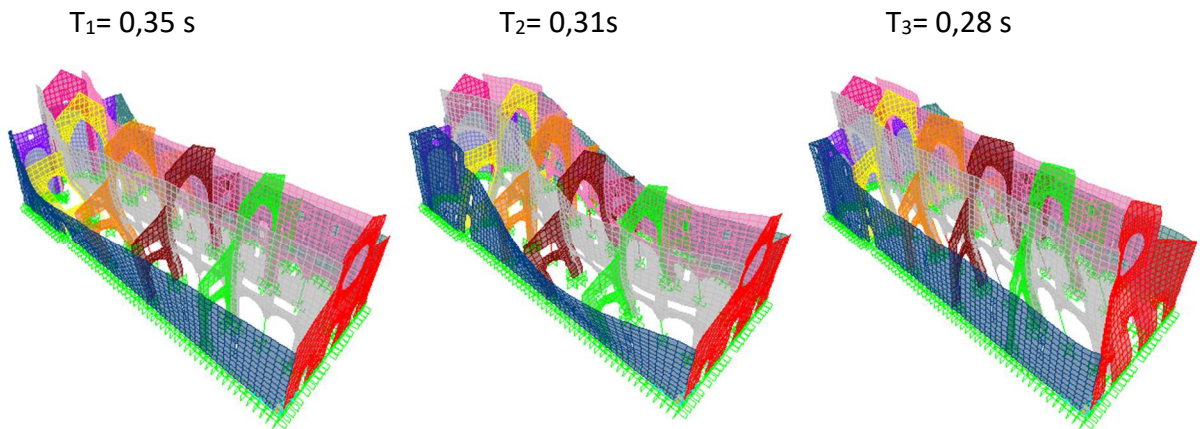
Fig. 17 *The first three modes of vibration of the Modena Cathedral FE model* [50] *(the 1st mode is responsible for damages in vault V2).*

Figure 18 compares the intrados cracks of the tested vault with the post-earthquake intrados cracks observed in the vault of the nave next to the façade (V1). A similar pattern is observed: (i) two "opening" cracks formed on two adjacent webs at 45° with respect to the diagonal rib, (ii) sliding cracks along the ribs. The weakness is in both cases along the bed joints and the cracks start from the diagonal ribs spreading on the adjacent webs.

20
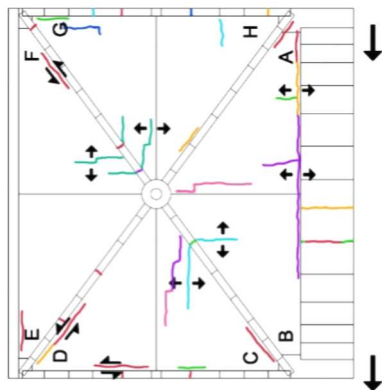
(a)   (b)   (c)

***Fig. 18:*** *Comparison between (a) the intrados of the tested vault and (b,c) the post-earthquake cracks observed in the intrados of the Modena Cathedral façade vault V1. The rigid edge is considered to lie along the rose window.*

Finally, it is worth pointing out that a similar structural response caused the collapse of two vaults in Saint Francis Basilica in Assisi (1997 Umbria earthquake), being these two vaults in the same boundary conditions as the tested one. The first was connected to the façade, the second to the rigid zone of the transept/apses [51].
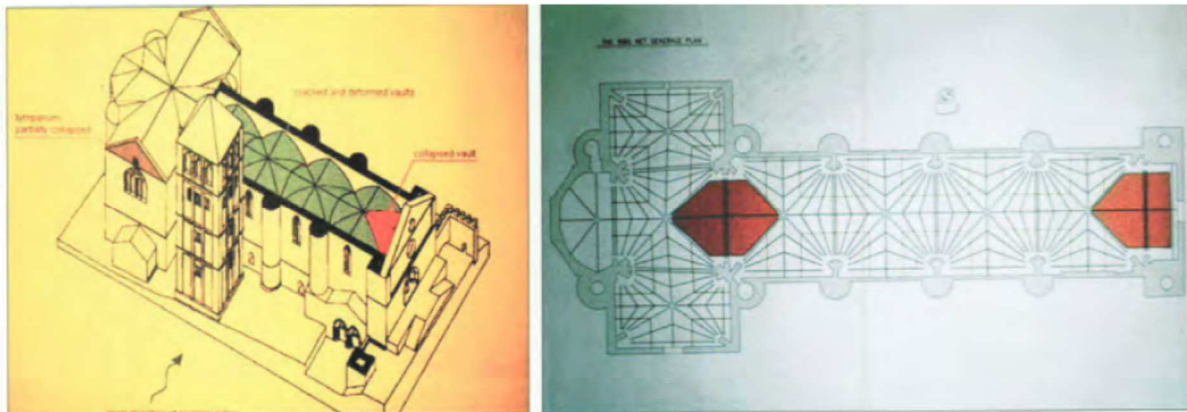
Fig. 19: *Damages incurred during the 1997 earthquake in the San Francesco church in Assisi* [51].

6   Conclusions

Historical churches, and specifically their masonry vaults, can be prone to seismic damage. Typically, in-plane shear deformation mechanisms occur in the vaults due to the large difference in the lateral stiffness between the piers of the nave and the longitudinal wall or the façade.

21

The interpretation through an experiment on 1:4 scaled specimen of a Gothic cross vault subjected to shear deformation at two if its springings confirmed the initiation of cracks normal to the diagonal ribs, showing that failure happens essentially at 2.7% spread of the longitudinal span, which is in good agreement with the few results on similar cases available in the scientific literature.

The linear and non-linear FE simulations to validate the test confirmed further aspects of the responses of the model, like the uplift of the vault, the shear deformation along the ribs and the asymmetric deformation (rotation). This confirms real case observations like in Saint Francis church in Assisi (1997 Umbria earthquake), San Marco in L'Aquila (2009 L'Aquila earthquake) and in Modena Cathedral (2012 Emilia earthquake), and can help distinguishing the origins of cracks observed in such buildings during their life span.

This validation can be followed by further tests of model vaults under proper dynamic conditions or the application of FRP reinforcement at the extrados to understand if this shear deformation mechanism can be halted.

References

[1]   S. Lagomarsino, "Damage assessment of churches after L'Aquila earthquake (2009)," *Bull. Earthq. Eng.*, vol. 10, no. 1, pp. 73–92, 2012.

[2]   S. Cattari, S. Resemini, and L. Sergio, "Modelling of vaults as equivalent diaphragms in 3D seismic analysis of masonry buildings," in *Structural Analysis of Historic Construction – D'Ayala & Fodde (eds)*, 2008.

[3]   S. Lagomarsino and S. Podestà, "Seismic vulnerability of ancient churches: I. Damage assessment and emergency planning," *Earthq. Spectra*, vol. 20, no. 2, pp. 377–394, 2004.

[4]   S. Baraccani *et al.*, "A Structural Analysis of the Modena Cathedral," *Int. J. Archit. Herit.*, vol. 3058, no. June, p. 15583058.2015.1113344, 2015.

[5]   A. Tralli, C. Alessandri, and G. Milani, "Computational Methods for Masonry Vaults: A Review of Recent Results," *Open Civ. Eng. J.*, vol. 8, no. 1, pp. 272–287, 2014.

[6]   P. Roca, M. Cervera, G. Gariup, and L. Pela', "Structural analysis of masonry historical constructions. Classical and advanced approaches," *Arch. Comput. Methods Eng.*, vol. 17, no. 3, pp. 299–325, 2010.

[7]   M. Como, *Statics of Historic Masonry Constructions*. .

[8]   E. Milani, G. Milani, and A. Tralli, "Limit analysis of masonry vaults by means of curved shell finite elements and homogenization," vol. 45, pp. 5258–5288, 2008.

[9]   A. Chiozzi, G. Milani, and A. Tralli, "A Genetic Algorithm NURBS-based new approach for

1   fast kinematic limit analysis of masonry vaults. No Title," *Comput. Struct.*, pp. 187–204,
2   2017.

3   [10]   G. Milani, "Upper bound sequential linear programming mesh adaptation scheme for
4   collapse analysis of masonry vaults," *Adv. Eng. Softw.*, vol. 79, pp. 91–110, 2015.

5   [11]   G. Milani and A. Tralli, "A simple meso-macro model based on SQP for the non-linear
6   analysis of masonry double curvature structures," *Int. J. Solids Struct.*, vol. 49, no. 5, pp.
7   808–834, 2012.

8   [12]   J. Heyman, *The stone skeleton:structural engineering of masonry architecture*. Cambridge
9   University Press, 1995.

10   [13]   P. Block and L. Lachauer, "Three-Dimensional (3D) Equilibrium Analysis of Gothic
11   Masonry Vaults," *Int. J. Archit. Herit.*, vol. 8, no. 3, pp. 312–335, 2014.

12   [14]   P. Block, T. Ciblac, and J. Ochsendorf, "Real-time limit analysis of vaulted masonry
13   buildings," *Comput. Struct.*, vol. 84, no. 29–30, pp. 1841–1852, 2006.

14   [15]   L. De Lorenzis, M. DeJong, and J. Ochesendorf, "Failure of masonry arches under impulse
15   base motion," *Earthq. Eng. Struct. Dyn.*, no. June, pp. 2119–2136, 2007.

16   [16]   L. Ferrario, M. Alessandra, V. Andreis, S. Zanotti, P. Riva, and E. Giuriani, "Behavior and
17   retrofitting of single-leaf vaults under distributed horizontal forces," in *Structural Analysis of
18   Historical Constructions –*, 2012.

19   [17]   E. E. Shapiro, "Collapse mechanisms of small-scale unreinforced masonry vaults," 2012.

20   [18]   T. Van Mele, J. McInerney, M. J. DeJong, and P. Block, "Physical and Computational
21   Discrete Modelling of Masonry Vault Collapse," *Struct. Anal. Hist. Constr. Vols 1-3*, pp.
22   2552–2560, 2012.

23   [19]   D. Theodossopoulos, B. P. Sinha, and a. S. Usmani, "Case Study of the Failure of a Cross
24   Vault: Church of Holyrood Abbey," *J. Archit. Eng.*, vol. 9, no. 3, pp. 109–117, 2003.

25   [20]   D. Theodossopoulos, N. Makoond, and L. AKL, "The Effect of Boundary Conditions on the
26   Behaviour of Pointed Masonry Barrel Vaults: Late Gothic Cases in Scotland," *Open Constr.
27   Build. Technol. J.*, vol. 10, no. Suppl 2: M8, pp. 274–292, 2016.

28   [21]   D. Theodossopoulos, J. Sanderson, and M. Scott, "Strengthening Masonry Cross Vaults
29   Damaged by Geometric Instability," in *Key Engineering Materials*, 2014, vol. 624, no.
30   January 2015, pp. 635–643.

31   [22]   G. Milani, M. Rossi, C. Calderini, and S. Lagomarsino, "Tilting plane tests on a small-scale
32   masonry cross vault: Experimental results and numerical simulations through a
33   heterogeneous approach," *Eng. Struct.*, vol. 123, pp. 300–312, 2016.

34   [23]   G. Rossi, M., Calderini, C., Lagomarsino, S., and Milani, "Seismic response of masonry
35   vaulted structures : experimental and numerical modelling.," in *9th International Masonry
36   Conference*, 2014.

37   [24]   A. Gaetani, "Seismic Performance of Masonry Cross Vaults : Learning from Historical
38   Developments and Experimental Testing," 2016.

23

[25] D. Theodossopoulos, "Structural behaviour of historic masonry cross vaults," 2002.

[26] D. Theodossopoulos, "The catastrophic repairs of Holyrood Abbey church in 1760," *Int. J. Archit. Herit.*, pp. 954–974, 2016.

[27] T. Bunyan, J. A. Faihurst, A. Mckie, and A. Macmillan, *Building stones of Edinburgh.* 1987.

[28] C. Carmela, B. Simonetta, and S. Stefano, "Pseudo-static response of masonry cross vaults to imposed shear displacements at the springings."

[29] G. Croci and F. Viskovic, A. Sabbadini, "Some Aspects of the Structural Behaviour of Gothic Cathedrals," in *Spatial structures: past, present and future, Milan: IASS*, 1995.

[30] P. Roca, L. Pellegrini, E. Oñate, and A. Hanganu, "Analysis of the structure of Gothic cathedrals: application to Barcelona cathedral," *Struct. Anal. Hist. Constr. Possibilities Numer. Exp. Tech.*, pp. 231–258, 1998.

[31] P. . Lourenco and J. G. Rots, "Multisurface Interface Model for Analysis of Masonry Structures Article," *J. Eng. Mech.*, vol. 230–238, no. 123, pp. 1–23, 1997.

[32] J. G. Rots, *Structural masonry: An experimental/numerical basis for practical design rules.* 1997.

[33] S. V.Chaudhari and M. A. Chakrabarti, "Modeling of Concrete for Nonlinear Analysis using Finite Element Code ABAQUS," *Int. J. Comput. Appl.*, vol. 44, no. 7, pp. 14–18, 2012.

[34] L. Pelà, M. Cervera, and P. Roca, "An orthotropic damage model for the analysis of masonry structures," *Constr. Build. Mater.*, vol. 41, pp. 957–967, 2013.

[35] L. Berto, A. Saetta, R. Scotta, and R. Vitaliani, "An orthotropic damage model for masonry structures," *Int. J. Numer. Methods Eng.*, vol. 55, no. 2, pp. 127–157, 2002.

[36] P. . Lourenço, "Computational strategies for masonry structures," *Available at: http://www.narcis.nl/publication/RecordID/oai:tudelft.nl:uuid:4f5a2c6c-d5b7-4043-9d06-8c0b7b9f1f6f.*, 1996.

[37] P. B. Lourenco, R. De Borst, and J. G. Rots, "A plane stress softening plasticity model for orthotropic materials," vol. 40, no. January, pp. 4033–4057, 1997.

[38] E. Papa, "A unilateral damage model for masonry based on a homogenisation procedure," *Mech. Cohesive-frictional Mater.*, 1996.

[39] A. Zucchini and P. B. Lourenco, "A micro-mechanical model for the homogenisation of masonry," vol. 39, pp. 3233–3255, 2002.

[40] A. Giordano, E. Mele, and A. De Luca, "Modelling of historical masonry structures: Comparison of different approaches through a case study," *Eng. Struct.*, vol. 24, no. 8, pp. 1057–1069, 2002.

[41] A. M. D'Altri, G. Castellazzi, S. de Miranda, and A. Tralli, "Seismic-induced damage in historical masonry vaults: a case-study in the 2012 Emilia earthquake-stricken area," *J. Build. Eng.*, vol. 13, no. August, pp. 224–243, 2017.

[42]   M. Acito, C. Chesi, G. Milani, and S. Torri, "Collapse analysis of the Clock and Fortified towers of Finale Emilia, Italy, after the 2012 Emilia Romagna seismic sequence: Lesson learned and reconstruction hypotheses," *Constr. Build. Mater.*, vol. 115, pp. 193–213, 2016.

[43]   A. Bayraktar, A. Şahin, D. M. Özcan, and F. Yildirim, "Numerical damage assessment of Haghia Sophia bell tower by nonlinear FE modeling," *Appl. Math. Model.*, vol. 34, no. 1, pp. 92–121, 2010.

[44]   Abaqus, "Theory manual, version 6.12." 2014.

[45]   Y. Sümer and M. Aktaş, "Defining parameters for concrete damage plasticity model," *Chall. J. Struct. Mech.*, vol. 1, no. 3, pp. 149–155, 2015.

[46]   M. Valente and G. Milani, "Seismic assessment of historicak masonry towers in the north-east region of Italy," no. June, pp. 5–10, 2016.

[47]   J. H. Lee and G. L. Fenves, "Plastic-damage model for cyclic loading of concrete structures," *J. Eng. Mech.*, vol. 124, no. 8, pp. 892–900, 1998.

[48]   P. S. Lourenço, "Experimental and numerical issues in the modelling of the machanical behaviour of masonry," 1998.

[49]   A. Page, "The Biaxial Compressive Strength of Brick Masonry.," *Proc. Inst. Civ. Eng.*, vol. 71, no. 3, pp. 893–906, 1981.

[50]   S. Baraccani, S. Silvestri, M. Palermo, G. Gasparini, and T. Trombetti, "The Assessment of the Seismic Behaviour of the Cathedral of Modena , Italy," in *Second European Conference on Earthquake engineering and seismology*, 2014, pp. 1–12.

[51]   G. Basile, *Restauri in San Francesco ad Assisi: Il cantiere dell'utopia : studi, ricerche e interventi sui dipinti murali e sulle vetrate dopo il sisma del 26 settembre 1997.* Perugia, Italy: Quattroemme, 2007.